Extending Kinematic Rupture Generators to Multi-segment Geometries

Brendon Bradley, Jake Faulkner
University of Canterbury, Department of Civil and Envoronmental Engineering | brendon.bradley@canterbury.ac.nz

1. Introduction

Kinematic rupture generators are an essential component of simulation-based ground motion prediction used in probabilistic seismic hazard analysis, such as CyberShake. One important limitation of such simulation-based ground motion predictions to date has been the use of single-segment rupture geometries. This is incompatible with contemporary source models used in seismic hazard analysis with empirical ground motion predictions, which adopt multi-segment rupture geometries (e.g., California and New Zealand, NZ).
In this poster, we summarize a framework to generalize single segment kinematic rupture generators to arbitrarily complex multi-segment rupture geometries, particularly targeted for use in national seismic hazard model (NSHM) applications.

2. Framework for generalizing from single- to multi-segment kinematic rupture generation

There are three key aspects that are required to extend from a single-segment kinematic rupture generator to multi-segment geometries, which is illustrated in Figure 1.

- ***Moment partitioning:*** What is the seismic moment on segment *i*, $M_{0,i}$, as a function of segment properties such as the segment area, A_i.
- ***Rupture path***: How the rupture propagates over the multiple segments in a macro-sense, i.e., which other segment initiates rupture on segments other than that with the hypocenter. For simple geometries, such as Figure 1, it is self-evident that Segment 2 is initiated by Segment 1, but more general rules are needed for arbitrarily-complex geometries.
- ***Jumping locations and time delay***: Given the general rupture path, what are the specific locations where jumping occurs between segments, and the associated time delay, e.g., the the point of rupture initiation on Segment 2, r_2, its conjugate point, r_2', on the initiating Segment 1, and the time delay between when rupture occurs at these two points as a function of the jump distance, $t_2(r_2)$.

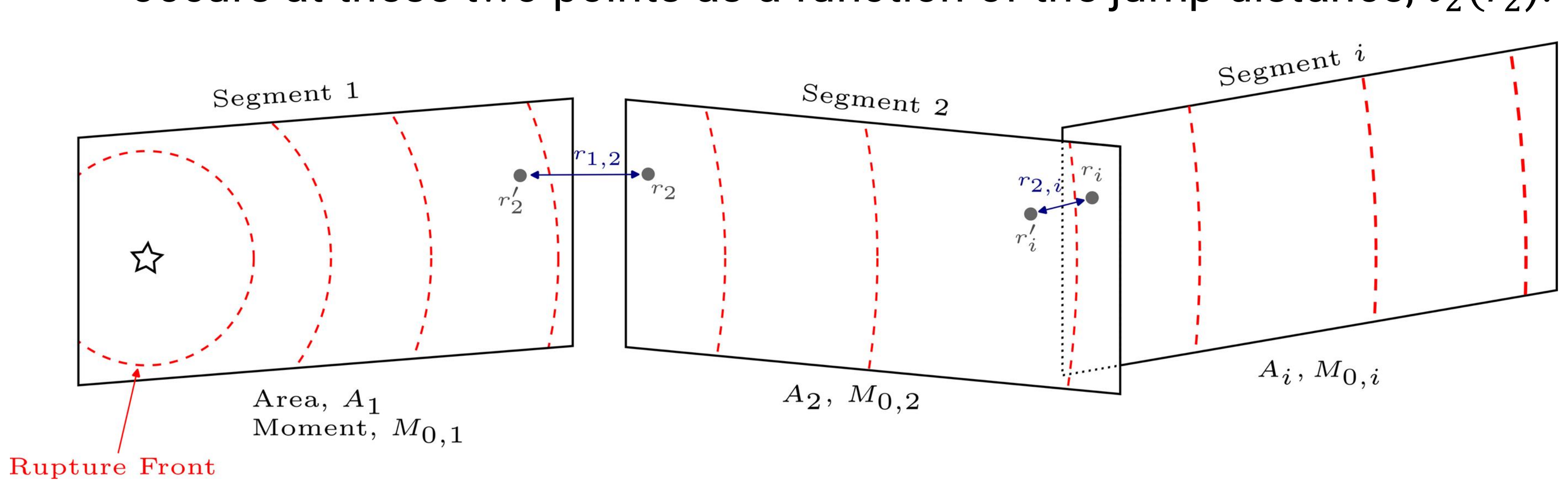

Figure 1: Schematic illustration of multi-segment rupture geometry illustrating the three components to generalize: (i) *moment partitioning* between segments; (ii) *rupture path* from the hypocenter; and (iii) *jumping locations* and *time delay*.

3. Calibration of framework parametrization

We used the SRCMOD database on kinematic source inversions to provide historical data to calibrate the three components of the multi-segment generalization. We also tested the calibrated model for complex rupture geometries in historical NZ earthquakes (specifically the 2010 Darfield and 2016 Kaikoura earthquakes), as well as application to prospective multi-segment ruptures from the 2022 NZ NSHM to understand its ability to generalize beyond the calibration dataset.

3.1. Moment partitioning

Kinematic rupture generation for single segments typically adopts a seismic moment, M_0, based on a $M_w - A$ scaling relation. When applied to a multi-segment rupture we adopt the same scaling relations using the total area, $A_T = \sum A_i$.

An important question is therefore *how is the total moment partitioned over all segments?*
Figure 2 illustrates empirical results from multi-segment ruptures in the SRCMOD database. There is scatter, but it supports a direct relationship of scaling with $A_i^{3/2}$ – implying unequal average slip displacement over all segments. Unequal slip displacement by segment also means that how segments are delineated is important.

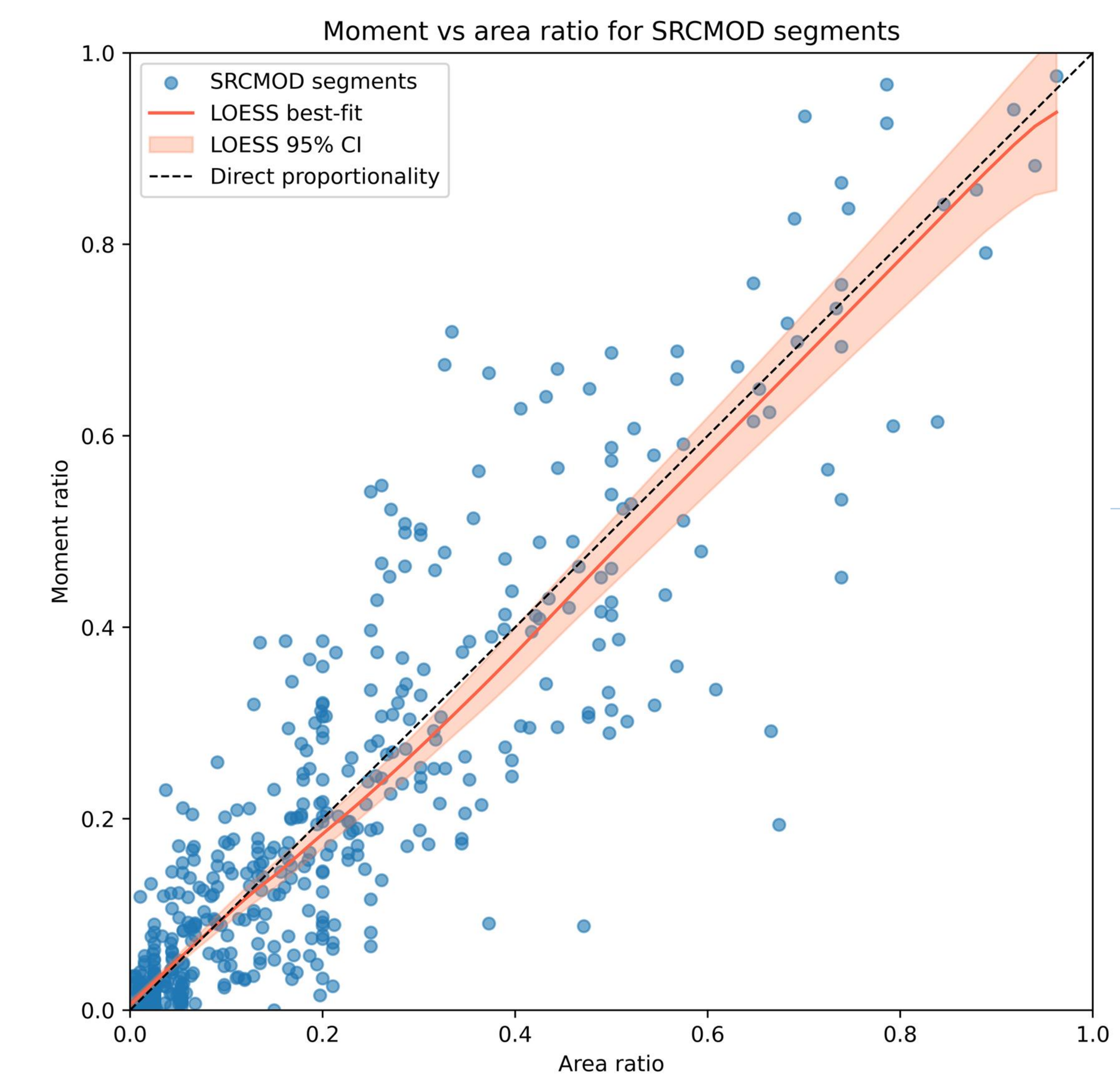

Figure 2: Empirical relationship between segment moment ratio, $M_{0,i}/M_{0,T}$, and area ratio, $A_i^{3/2}/\sum A_i^{3/2}$.

3.2. Rupture path

A *probability tree* for the rupture path, from a defined hypocenter, is developed based on an exponential decay of rupture probabilities, $P(S_i \text{ triggers } S_j) = e^{-r_{ij}/r_o}$, where $r_0 = 3$ km. We then can sample the probability true to develop a stochastic representation of possible rupture paths:

$$P(T) \propto \prod_{(S_i,S_j)\in T} P(S_i \text{ triggers } S_j) \prod_{(S_i,S_j)\notin T} [1 - P(S_i \text{ triggers } S_j)]$$

Figure 3 illustrates examples of the rupture paths for the 2010 Darfield and 2016 Kaikoura earthquakes. In each of these cases there are minor differences among the alternative rupture paths which occur when 3+ fault planes exist in close proximity ('junctions'). However, these have a minimal impact on the actual location and timing of rupture initiation on each segment, and thus the resulting rupture.

Figure 4 illustrates an example of the application of the rupture path algorithm to a $M_w 8.5$ Alpine-Hope fault multi-segment rupture from the 2022 NZ NSHM. Most ruptures, even in complex contemporary source models, have only one viable rupture path in a macro sense.

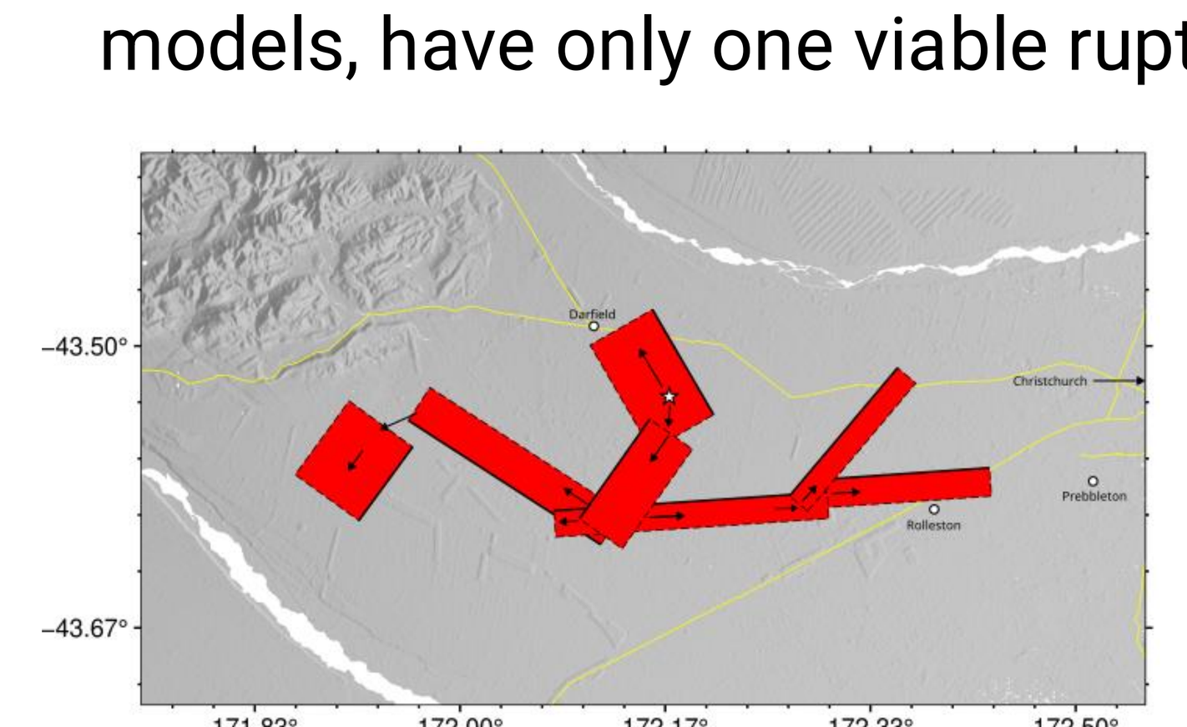

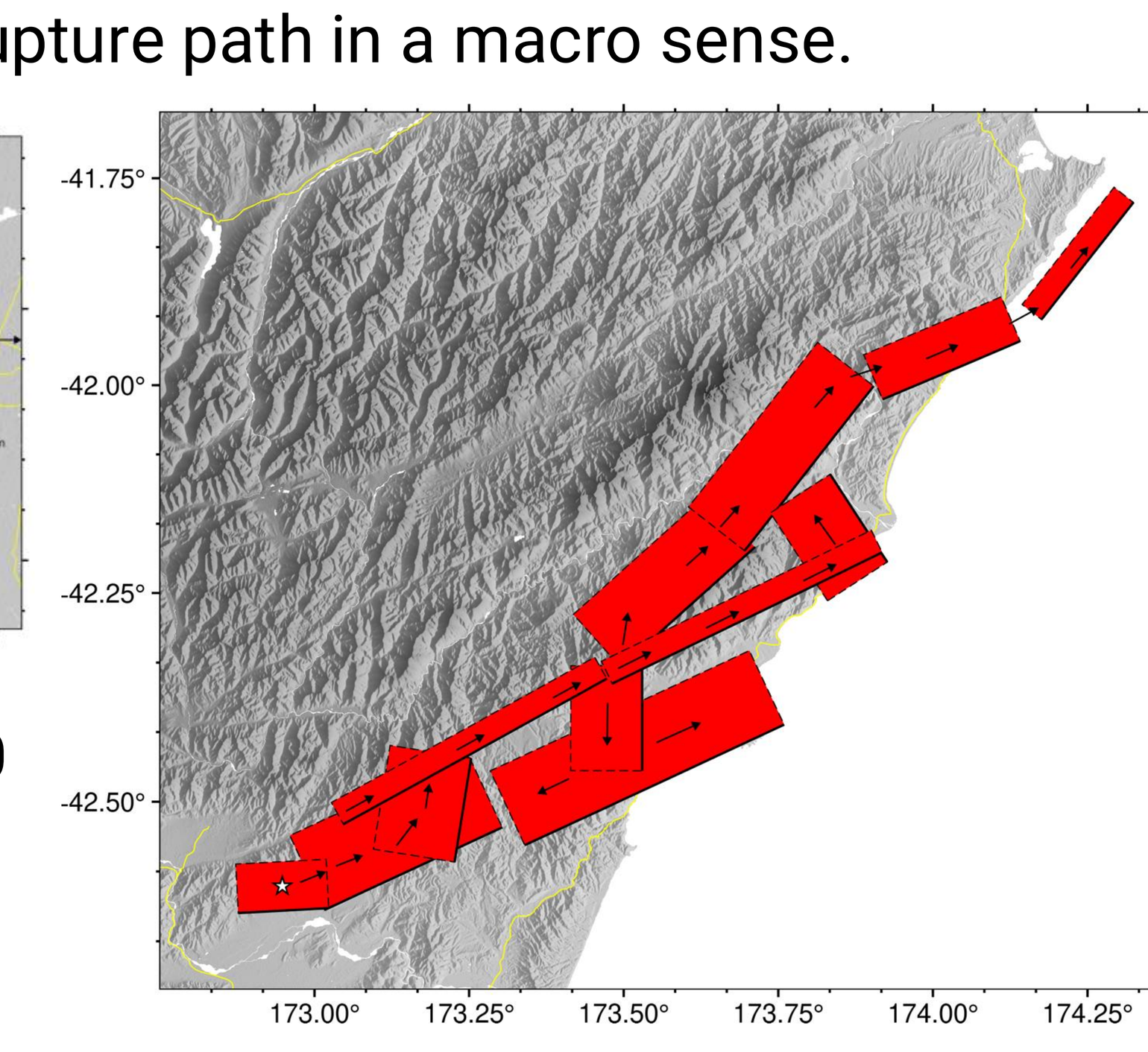

Figure 3: Examples from the 2010 Darfield (left) and 2016 Kaikoura (right) earthquake of the rupture path algorithm.

Figure 4: Rupture path of a $M_w 8.5$ Alpine-Hope fault geometry, which is from the 2022 NZ NSHM.

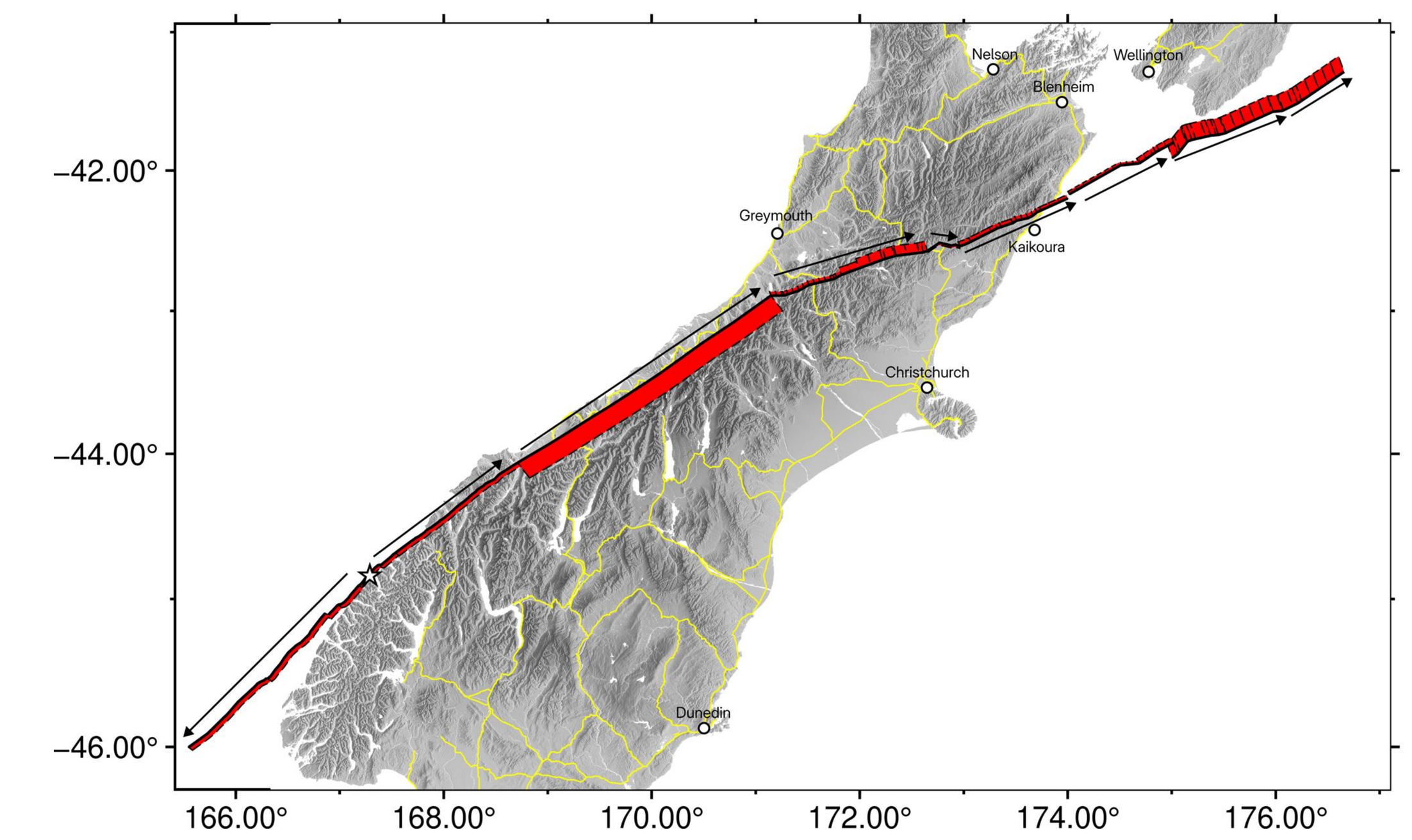

3.3. Jumping locations and time delay

We use the rupture causality tree determined by the rupture path algorithm. Between each pair of segments, (S_i, S_j), where segment S_i triggers S_j we perform an optimization process to identify the closest points between the two segments with a depth of at least five kilometers. The optimization of *L* depends on normalized along-strike and down-dip coordinates (s, d), and a natural embedding function, *F*.

$$L(s,d,s',d') = |F(s,d) - F(s',d')|$$

Figure 5 compares the locations of jumping in historical SRCMOD events based on inversion and this algorithm.

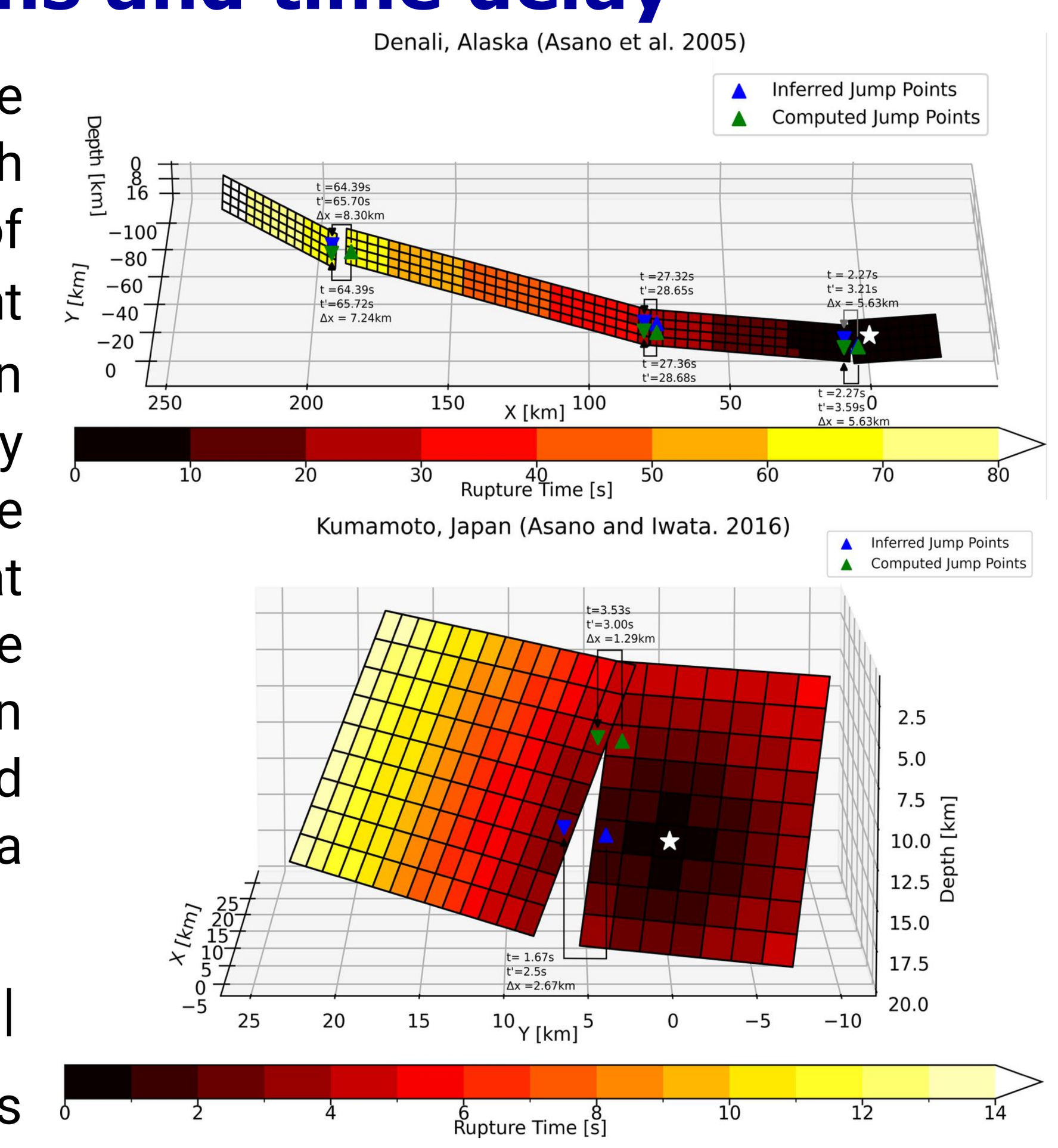

Figure 5: Historical SRCMOD database events comparing inferred and computed jump locations with our algorithm.

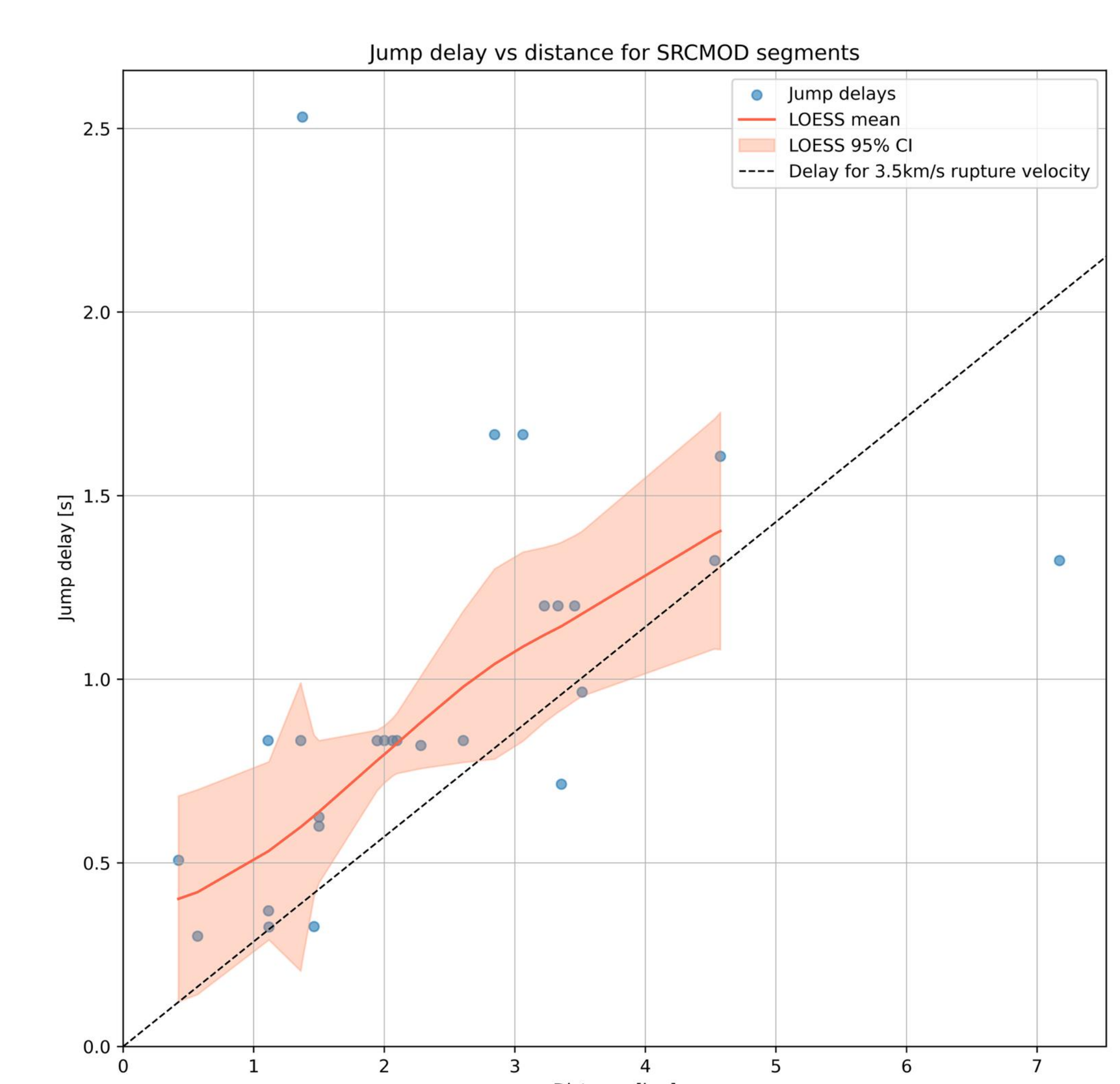

Figure 6 illustrates the time delay of rupture between segments calculated from events in the SRCMOD database as a function of separation distance.
The relationship is easily modeled as a function of the jump distance, the shear-wave velocity and a random perturbation.

$$\Delta t_{i,j} = \frac{r_{i,j}}{V_s} + \delta_{i,j}$$

Figure 6: Time delay of rupture jumping from multi-segment ruptures in the SRCMOD database

4. Rupture dynamics consistency

As with all kinematic rupture generations, we have been considering how the proposed multi-segment extensions are consistent with, or violate, rupture dynamics. Important considerations include:

- Conditions that give rise to non-equal slip over different segments.
- Rupture path probabilities that account for Coulomb stress
- Jump location and timing that is not over-sensitive to simple geometries